Original Article

Fast kilovoltage peak-switching dual-energy computed tomography water-hydroxyapatite decomposition for detecting vertebral compression fracture-related bone marrow edema: a comparison with magnetic resonance imaging

Rong Yao^, Xue'e Zhu^, Dan Zhou^, Li Yang^, Hanxiao Yu^, Rui Zhang^, Tongbo Yu^, Menghua Yang^

Department of Radiology, BenQ Medical Center, The Affiliated BenQ Hospital of Nanjing Medical University, Nanjing, China

Contributions: (I) Conception and design: X Zhu, R Yao; (II) Administrative support: D Zhou; (III) Provision of study materials or patients: H Yu, M Yang; (IV) Collection and assembly of data: L Yang, R Zhang, T Yu; (V) Data analysis and interpretation: X Zhu, R Yao; (VI) Manuscript writing: All authors; (VII) Final approval of manuscript: All authors.

Correspondence to: Xue'e Zhu, MD, PhD. Department of Radiology, BenQ Medical Center, The Affiliated BenQ Hospital of Nanjing Medical University, 71 Hexi Ave, Jianye District, Nanjing 210019, China. Email: snowy2009@126.com.

Background: Dual-energy computed tomography (DECT) material decomposition techniques have been reported to be effective for identifying acute and chronic vertebral compression fractures (VCFs) as compared with magnetic resonance imaging (MRI). However, a quantitative evaluation of the consistency of the bone marrow edema (BME) region depicted by DECT with that delineated by MRI has not been reported. This study thus aimed to qualitatively and quantitatively assess the fast kilovoltage peak (kVp)-switching DECT water-hydroxyapatite (HAP) decomposition technique in detecting traumatic BME in patients with VCFs and compare it to MRI.

Methods: A total of 195 consecutive patients who underwent both spinal DECT and MRI within 3 days from each other were retrospectively enrolled. All vertebral bodies were blindly evaluated for the presence of traumatic BME on water-HAP images. Water concentration was measured in all vertebral bodies, and the maximum area of BME was measured in the edematous ones. An experienced radiologist blindly evaluated the presence of BME on fluid-sensitive MR images, which served as the reference, and calculated the maximum area of BME. One-way analysis of variance with post hoc pairwise comparisons (Tamhane's T2 at $P<0.05$) was used to compare water concentrations among acute VCFs, chronic VCFs, and normal vertebrae. Receiver operating characteristic (ROC) curve analysis was conducted to predict acute VCFs. Bland-Altman analysis was performed to evaluate the consistency of the maximum area of BME measured on DECT and MRI.

Results: In the visual analysis of acute VCFs, water-HAP images had an overall sensitivity of 97.1%, a specificity of 99.7%, and an accuracy of 99.4%. Water concentration differed significantly between acute and chronic VCFs and between acute VCFs and normal vertebrae ($P<0.001$), but it did not differ significantly between chronic VCFs and normal vertebrae ($P=0.998$). ROC curve analysis yielded an area under the curve of 0.989, and the optimal threshold of 991.4 mg/cm^3 yielded a 94.9% sensitivity and a 90.3% specificity in identifying edematous vertebral bodies. Bland-Altman plots indicated that all mean differences in the maximum area of BME measured on DECT and MRI were nearly zero ($P>0.05$), with most differences having a standard deviation within 1.96.

^ ORCID: Rong Yao, 0009-0002-3847-7982; Xue'e Zhu, 0000-0003-2060-9078; Dan Zhou, 0000-0002-8961-5276; Li Yang, 0009-0006-4145-9979; Hanxiao Yu, 0009-0002-1733-1618; Rui Zhang, 0009-0009-7821-1055; Tongbo Yu, 0009-0003-0889-1733; Menghua Yang, 0009-0009-7915-3504.

Conclusions: The fast kVp-switching DECT water-HAP decomposition technique had an excellent diagnostic performance in distinguishing acute VCFs from chronic ones. The depicted areas of BME on DECT and MRI were highly similar.

Keywords: Dual-energy computed tomography (DECT); vertebral compression fracture (VCF); water-hydroxyapatite decomposition; bone marrow edema (BME); material decomposition

Submitted Aug 14, 2024. Accepted for publication Feb 10, 2025. Published online Feb 26, 2025.
doi: 10.21037/qims-24-1576
View this article at: https://dx.doi.org/10.21037/qims-24-1576

Introduction

Single-energy computed tomography (CT) of the spine is the standard examination for fast exclusion or for more in-depth assessment of suspected or known vertebral compression fractures (VCFs) (1-4). However, in some cases, such as minor fractures, occulted fractures, old fractures with recurrent fractures, and osteoporosis with fractures, single-energy CT is not able to distinguish between acute and chronic VCFs because it cannot directly reveal bone marrow edema (BME) (2). Fat-suppressed T2-weighted magnetic resonance imaging (MRI) is the gold standard imaging modality in distinguishing between acute and chronic fractures (5) due to its ability to depict BME caused by acute fractures (6). However, MRI has many contraindications and shortcomings, which may prevent some patients from receiving timely MRI examinations.

Dual-energy CT (DECT) is a promising imaging modality in the assessment of VCFs and possesses the advantages of both single-energy CT and MRI (in demonstrating BME). Previous investigations have evaluated the ability of DECT to identify BME in the spine based on material decomposition techniques (2,7-22). The virtual noncalcium (VNC) technique based on three-material decomposition was used in the bulk of these studies (2,9-17,19-22), while the two-material decomposition was applied in fewer studies (7,8,18). Both approaches demonstrated good performance in identifying acute and chronic VCFs as compared with MRI. However, to the best of our knowledge, a quantitative evaluation of the consistency of the BME region depicted by DECT with that delineated by MRI has not been conducted, and the extent to which DECT can serve as a substitute for MRI in diagnosing VCFs remains unknown.

The purpose of this study was thus to qualitatively and quantitatively assess the fast kilovoltage peak (kVp)-switching DECT water-hydroxyapatite [HAP; $Ca_{10}(PO_4)_6(OH)_2$] decomposition technique in detecting traumatic BME in patients with VCFs and to compare it with MRI. We present this article in accordance with the STARD reporting checklist (available at https://qims.amegroups.com/article/view/10.21037/qims-24-1576/rc).

Methods

Patients

The retrospective study was conducted in accordance with the Declaration of Helsinki (as revised in 2013) and was approved by the institutional ethics committee of the Affiliated BenQ Hospital of Nanjing Medical University (No. 2023-KL017). The requirement for written informed consent was waived due to the retrospective nature of the analysis. This study was conducted at the Affiliated BenQ Hospital of Nanjing Medical University. In total, 1,012 consecutive emergency patients with spinal trauma and orthopedic outpatients with recent lower back pain and suspected VCFs treated between December 2021 and June 2024 were enrolled in our study. The exclusion criteria were as follows: lack of spine DECT examination, lack of spine MRI within 3 days for correlation, spinal tumors, spinal infection, and basic diseases or drugs affecting calcium and phosphorus metabolism. The final study group consisted of 195 patients (mean age 64.1±13.6 years; age range 14–92 years), with 63 males and 132 females. Moreover, 8 vertebral bodies were excluded due to the presence of hemangiomas, and 18 were excluded due to a history of surgery for VCFs (*Figure 1*).

Image acquisition

CT scanning was performed using a single-source DECT system (Revolution Apex, GE HealthCare, Chicago, IL, USA). The acquisition parameters were as follows:

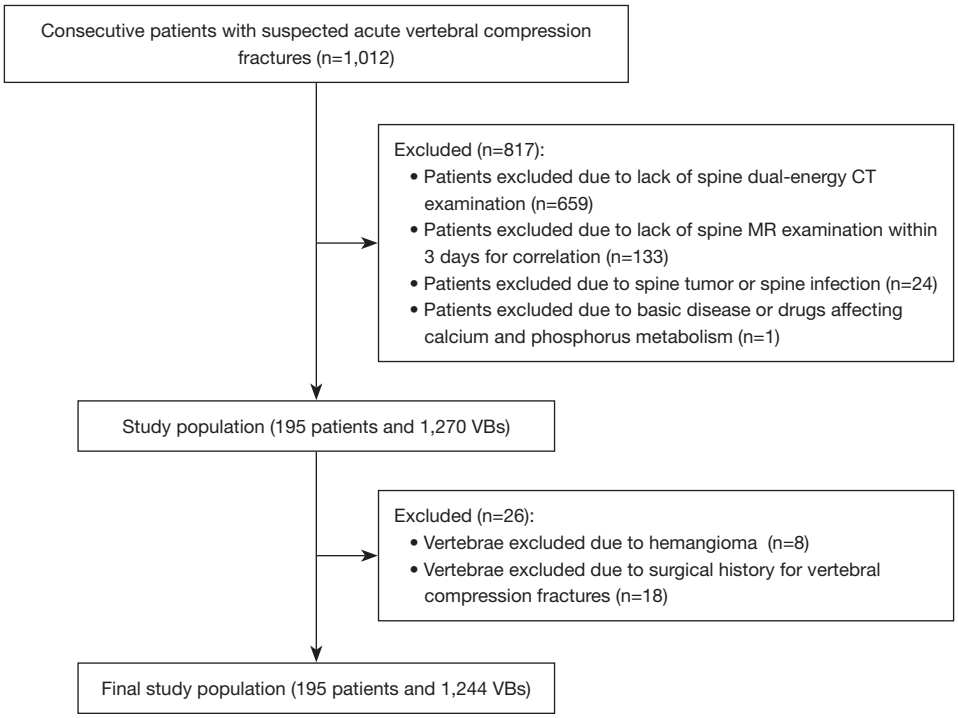

Figure 1 Inclusion and exclusion criteria. CT, computed tomography; MR, magnetic resonance; VBs, vertebral bodies.

gemstone spectral imaging (GSI) kilovoltage (kV) mode with rapid kV-switching between 80 and 140 kV, a tube current milliampere (mA) set by GSI assist with a noise index of 8.5, a collimation thickness of 0.625 mm, a helical scan type, a rotation time of 0.5 s, a helical pitch of 0.984, 60% adaptive statistical iterative reconstruction-V, and a data file standard reconstruction type.

MRI was conducted on a 1.5-T system (Intera; Philips Healthcare, Best, the Netherlands). All imaging was performed with a spine surface coil. Images were obtained using a sagittal T2-weighted spectral-attenuated inversion recovery (SPAIR) sequence (repetition time, 3,757 ms; echo time, 90 ms; slice thickness, 3.5 mm; gap, 3.5 mm; echo train length, 15; number of signal averages, 3).

Postprocessing

The data of the DECT images were postprocessed using an Advanced Workstation 4.7 (GE HealthCare). The water-HAP decomposition technique generated two types of images: the water-HAP image was generated by subtracting HAP, and the HAP-water image was obtained by subtracting water. For further analyses, color-coded overlay water-HAP images were generated by merging the water-HAP images with the data file's CT images.

Image analysis

MR images of the spine were displayed separately in a random manner and visually analyzed by an experienced radiologist (X.Z., with 20 years of experience in musculoskeletal radiology). This reader blindly and independently assessed whether each vertebra had traumatic BME and morphologic compression. The vertebral bodies with traumatic BME were classified as acute VCFs, while the vertebral bodies without traumatic BME but with morphologic compression were classified as chronic VCFs. The vertebral bodies with neither traumatic BME nor morphologic compression were considered to be normal vertebral bodies. For acute VCFs, the maximum area of the BME (ma-BME) was calculated by drawing a region of interest (ROI) on sagittal T2-weighted SPAIR images (*Figure 2A*,*2B*).

Two radiologists [L.Y. (reader 1) and R.Y. (reader 2), with 10 and 15 years of experience in musculoskeletal radiology, respectively] were blinded to the MRI results and analyzed DECT images in a randomized fashion. First, the two readers independently evaluated each vertebral body

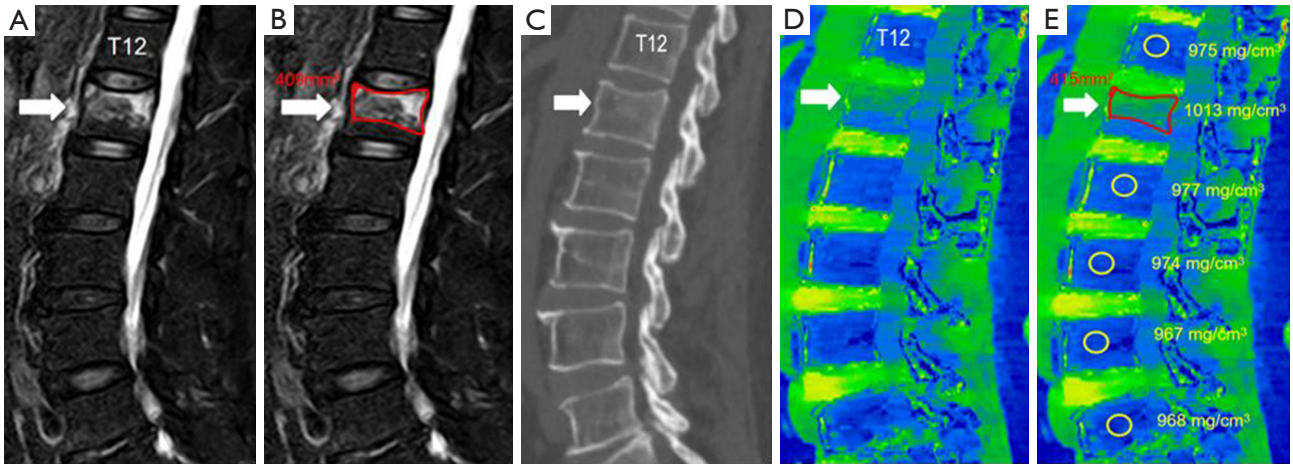

Figure 2 Images of a 63-year-old woman with a compression fracture of uncertain age at L1. Sagittal T2-SPAIR of the lumbar (A,B) showing BME of the L1 vertebral body (arrow) confirming the presence of an acute compression fracture, wherein the maximum area (red outline in B, mm^2) was measured. Sagittal weighted-average CT image of the lumbar spine in the bone window setting (C) showing the anterior cortex slightly distortion of L1 vertebral body without interruption (arrow), and L1 vertebral body being slightly decreased in height. Corresponding color-coded DECT water (HAP) image (D,E) displayed BME within the L1 vertebral body (arrow) compatible with an acute compression fracture, wherein the maximum area (red outline in E, mm^2) and the water concentration (mg/cm^3) corresponding to the area were measured. No more vertebral compression fractures were found. The ROIs were placed randomly in the middle of the normal vertebral bodies (yellow circles in E, area =100 mm^2) and the water concentration (mg/cm^3) corresponding to the area were measured. SPAIR, spectral attenuated inversion recovery; BME, bone marrow edema; CT, computed tomography; DECT, dual-energy computed tomography; HAP, hydroxyapatite; ROI, region of interest.

for the presence of morphologic fractures on weighted-average CT images (*Figure 2C*). The vertebral bodies with cortical fractures were classified as acute VCFs. The vertebral bodies without cortical fractures but with morphologic compression were classified as chronic VCFs. The vertebral bodies with neither cortical fractures nor morphologic compression were considered normal vertebral bodies. Second, the two readers independently evaluated each vertebral body for the presence of BME, which was represented as green on color-coded DECT water-HAP images (*Figure 2D*). The vertebral bodies with BME were classified as acute VCFs. The vertebral bodies without BME but with morphologic compression were classified as chronic VCFs. The vertebral bodies with neither BME nor morphologic compression were classified as normal vertebral bodies. If the two readers disagreed, consensus was reached through joint reading.

Quantitative image analyses were performed following the application of the visual analysis performed by two radiologists (L.Y. and R.Y.) based on the sagittal plane. For acute VCFs, the ma-BME was measured on the sagittal color-coded water-HAP images, and the water concentration corresponding to the area was obtained (*Figure 2E*). In the chronic VCFs and normal vertebral bodies that were presented in blue on color-coded water-HAP images, the ROI was placed randomly in the middle of the vertebral body. In clinical practice, the ROIs should be as large as possible to better reflect the information of the measured vertebral body and should be at least 2 mm distant from the cortical bone to avoid central veins or bone islands. In addition, we ultimately set the measurement range as 100 mm^2 (*Figure 2E*) according to Petritsch *et al.*'s work (19).

The readers could freely scroll through the water-HAP images displayed in the standard window settings (center: 1,000 mg/cm^3; width: 300 mg/cm^3) and adjust the window settings according to personal preference.

Statistical analysis

Continuous variables are expressed as the mean ± standard deviation (SD). MRI served as the gold standard. For visual analyses, we drew a contingency table to calculate the sensitivity, specificity, accuracy, and predictive values. For

Table 1 Contingency table of vertebral bodies for subjective image analyses

Traumatic BME on MRI	Cortical fracture on CT		No cortical fracture on CT	
	BME on DECT	No BME on DECT	BME on DECT	No BME on DECT
Traumatic BME	115	0	17	4
No traumatic BME	0	13	3	1,092

Data are the numbers of vertebral bodies. BME, bone marrow edema; MRI, magnetic resonance imaging; CT, computed tomography; DECT, dual-energy computed tomography.

quantitative analyses, one-way analysis of variance (ANOVA) with post hoc pairwise comparisons (Tamhane's T2 at $P<0.05$) was used to compare the water concentrations between acute VCFs, chronic VCFs, and normal vertebrae. Additionally, receiver operating characteristic (ROC) curve analysis was performed, and the threshold of water concentration was calculated to predict acute VCFs. Moreover, Bland-Altman analysis was performed to evaluate the consistency of the ma-BME measured on DECT and MRI. SPSS version 23.0 (IBM Corp., Armonk, NY, USA) and MedCalc version 19.6.4 (MedCalc Software Ltd., Ostend, Belgium; https://www.medcalc.org; 2021) were used for statistical analyses. $P<0.05$ was considered statistically significant.

Results

In this study, 1,244 vertebrae among 195 patients were examined. The MRI results indicated 136 (10.9%) acute VCFs in 121 patients with BME, 110 (8.9%) chronic VCFs in 68 patients, and 998 (80.2%) normal vertebral bodies.

Among the patients, 77 had only acute VCF, 21 had only chronic VCF, 44 had both acute and chronic VCF, and 53 had neither acute nor chronic VCF. With respect to acute VCFs (45 thoracic and 91 lumbar vertebrae), 108 patients had one acute VCF, while 13 had two or three acute VCFs.

Visual image analysis

In total, 115 true-positive acute VCFs, 13 false-positive findings (chronic VCFs), 1,095 true-negative findings (97 chronic VCFs and 998 normal vertebrae), and 21 false-negative findings were found based on the weighted-average CT images (*Table 1*). Among the 115 cases of acute VCF identified by weighted-average CT images, all types (A1–A4 of the Arbeitsgemeinschaft für Osteosynthesefragen spinal classification system) of compression injuries were examined, including 63 cases of A1 type, 31 cases of A2 type, 12 cases of A3 type, and 9 cases of A4 type. Of the 136 acute VCFs, 21 were underdiagnosed on the basis of the weighted-average CT images due to the lack of cortical interruption, while 17 were identified with the help of DECT color-coded water-HAP images. As a result, 132 true-positive acute VCFs and 4 false-negative findings were identified on DECT color-coded water-HAP images. Of the 110 chronic VCFs, 13 were misdiagnosed as acute based on the weighted-average CT images, whereas 11 were corrected with the help of DECT color-coded water-HAP images. One normal vertebra was misdiagnosed as acute VCF on DECT color-coded water-HAP images. Three false-positive findings (two chronic VCFs and one normal vertebra) and 1,105 true-negative findings were found on DECT color-coded water-HAP images (*Table 1*). The DECT color-coded water-HAP images had an overall sensitivity of 97.1%, a specificity of 99.7%, an accuracy of 99.4%, a positive predictive value of 97.8%, and a negative predictive value of 99.6%.

Quantitative water-HAP image evaluation

Significant differences in the water concentration on DECT color-coded water-HAP images were found between acute and chronic VCFs ($P<0.001$) and between acute VCFs and normal vertebrae ($P<0.001$). The difference in water concentration between chronic VCFs and normal vertebrae was not statistically significant ($P=0.998$; *Table 2*).

The ROC curve analysis of the water concentration indicated an area under the curve (AUC) of 0.989 (*Figure 3*). The optimal threshold for water concentration obtained using the Youden index was 993.0 mg/cm^3, with a corresponding sensitivity and specificity of 91.2% and 95.5%, respectively. From a clinical perspective, we aim to achieve a DECT sensitivity sufficiently high to minimize the misdiagnosis rate of acute vertebral fractures and avoid delaying patient treatment. Therefore, we selected an optimal threshold of 991.4 mg/cm^3 based on the optimal

Table 2 Comparison of vertebral body water concentration measured on DECT water (HAP) images among different groups*

Vertebral bodies	Water concentration (mg/cm^3)
Acute VCFs (n=136)	1,006.9±9.2 (985.0–1,031.0)
Chronic VCFs (n=110)	977.6±11.6 (943.6–1,004.0)
Normal vertebrae (n=998)	977.4±11.0 (928.0–1,003.0)
P values*	
Acute *vs.* chronic VCFs*	<0.001
Acute *vs.* normal vertebrae*	<0.001
Chronic *vs.* normal vertebrae*	0.998

Data are presented as mean ± standard deviation (range). *, Tamhane's T2 test was used for all pairwise comparisons due to heterogeneity of variance. DECT, dual-energy computed tomography; HAP, hydroxyapatite; VCFs, vertebral compression fractures.

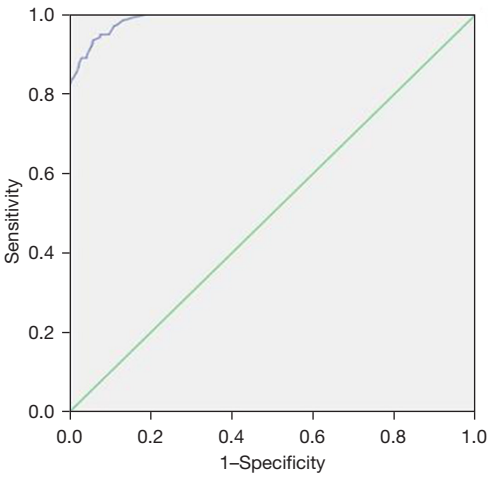

Figure 3 ROC curves calculated from the water concentration derived from DECT water (HAP) images for the differentiation of vertebral bodies with and without BME. Area under the curve was 0.989. ROC, receiver operating characteristic; DECT, dual-energy computed tomography; HAP, hydroxyapatite; BME, bone marrow edema.

sensitivity. Under this, the corresponding sensitivity and specificity in differentiating edematous vertebral bodies from non-edematous ones were 94.9% and 90.3%, respectively.

Bland-Altman plots indicated no significant differences in the ma-BME measured on DECT and MRI (P=0.893), and the ma-BME values measured on DECT and MRI were

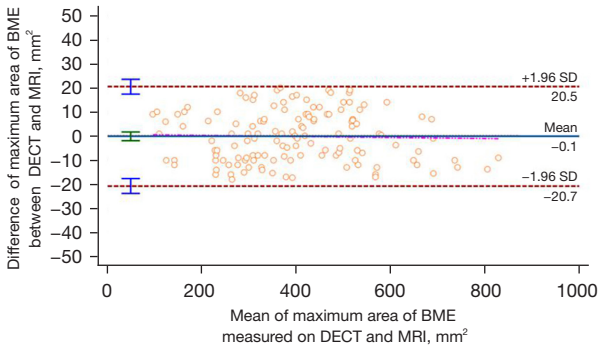

Figure 4 Bland-Altman plots showing high agreement on the maximum area of BME between measurements on DECT and MRI. All mean differences were nearly zero (P>0.05). Most of the differences lay between ±1.96 SD. BME, bone marrow edema; DECT, dual-energy computed tomography; MRI, magnetic resonance imaging; SD, standard deviation.

highly consistent. All mean differences were nearly zero, with the majority being within an SD of 1.96 (*Figure 4*).

Discussion

In this study, with MRI serving as the gold standard, we found that the fast kVp-switching DECT water-HAP technique had an excellent diagnostic performance for identifying and characterizing traumatic BME in acute thoracolumbar VCFs, both visually and quantitatively.

The fast kVp-switching DECT system adopts a single X-ray source, which can quickly change the energy setting and collect data with low-energy and high-energy scans during each rotation. The principle of the DECT two-material decomposition technique is that attenuation measurements at tube voltages of low and high kilovolts can be subjected to two-material decomposition, allowing for the mathematical subtraction of substances with a relevant photograph-electric effect. Compared with three-material decomposition, two-material decomposition is more widely used in clinical practice, including in virtual nonenhanced CT, CT angiography decalcification, and gout screening, among others. In addition, two-material decomposition techniques can be performed on any manufacturer's DECT device, while three-material decomposition techniques (VNC) require specific postprocessing software, which is not available on some DECT devices. The key to successfully performing the two-material decomposition technique is to select two suitable base substances. Usually,

the two components with higher content in the structure are selected as the base substances. Liao *et al.* demonstrated that HAP is the main mineral component of bone and is more similar to the true bone mineral composition than is calcium (23). When acute VCFs occur, trabecular microfractures, edema, and hemorrhage following trauma lead to increased amounts of interstitial fluid and blood that cause an increase in the water concentration (24,25). Due to these two reasons, we selected water-HAP images to virtually subtract the HAP concentration that had the highest content in the bone marrow cavity and to display the water concentration that had the greatest change when acute VCFs were present.

Thus far, only a few studies have examined the use of the two-material decomposition technique to visualize BME in the spine, pelvis, or upper and lower extremities (7,8,18,26). Pan *et al.* were the first to report on the detection of posttraumatic bone marrow lesions in the spine with the use of fast kVp-switching DECT water-HAP images (18). In their study, the water concentration of BME in acute VCFs was significantly higher than that in chronic VCFs (1,015.8±11.9 *vs.* 997.0±9.3 mg/cm^3; P<0.001), and our study produced similar results (1,006.9±9.2 *vs.* 977.6±11.6 mg/cm^3; P<0.001). The ROC for differentiating edematous vertebral bodies from non-edematous ones in our study yielded an AUC of 0.989, which is similar to the 0.917 obtained by Pan *et al.*; moreover, the optimal cutoff value of 991.4 mg/cm^3 (94.9% sensitivity and 90.3% specificity) in our study was similar to the 1,003.2 mg/cm^3 value (88.9% sensitivity and 82.9% specificity) reported by Pan *et al.* Meanwhile, the high sensitivity (94.9%) and specificity (90.3%) of the optimal threshold for detecting traumatic BME support the quantitative analysis of DECT water-HAP images as a valuable means for diagnosing and identifying chronic and acute VCFs. In addition, the high negative predictive value of 99.6% in the visual analysis confirmed the feasibility of using DECT water-HAP images to exclude acute VCFs.

Furthermore, our investigation revealed that the ma-BME values measured on DECT water-HAP images and on MRI were highly consistent. Until this study, the ability to measure the BME area via DECT water-HAP images and MRI had not been quantitatively compared. Almost all the studies in this area have focused on the qualitative assessment of BME through two- or three-material decomposition techniques (2,7-11,14-22). Our quantitative findings demonstrated that there is high consistency between DECT water-HAP images and MRI T2-weighted SPAIR images in delineating the area of traumatic BME in acute VCFs. When acute VCF occurs, edema and hemorrhage cause an increase in the water concentration (24,25). MRI T2-weighted SPAIR images can reflect the presence of free water, and the DECT water-HAP images can reflect the increase in the water concentration due to the presence of free water. The underlying principles of these approaches are similar. MRI is the gold standard imaging modality for differentiating between acute and chronic fractures. We found that the DECT water-HAP decomposition technique can quickly depict the areas of BME with almost the same accuracy as that of MRI. Therefore, radiologists may have more confidence in effectively identifying acute VCFs with the help of water-HAP images without MRI. Despite MRI being the preferred imaging modality for distinguishing between acute and chronic VCFs, it is sometimes not suitable for emergency cases who cannot remain still during the longer scan time or for those with contraindications to MRI. In such cases, DECT can replace MRI for examination. In emergency situations, the DECT water-HAP decomposition technique can serve as a diagnostic tool to quickly exclude or confirm acute VCFs—as it has high sensitivity and specificity—and it can allow clinicians to forego additional MRI examinations, enabling timely and appropriate clinical management. However, this does not mean that DECT can completely replace MRI or other imaging modalities. Compared to MRI, DECT entails a greater radiation hazard, and compared to plain scans, involves a higher radiation dose. Additionally, compared to traditional CT machines, DECT machines are more expensive, and for these reasons, primary healthcare institutions face difficulty in consistently performing DECT.

Despite the promising results, three false-positive findings and four-false negative findings were observed in visual image interpretation. All three false-positive results (two chronic VCFs and one normal vertebra) were associated with the Modic type 1 vertebral endplate change, and all occurred in emergency patients with back pain after trauma. The areas of Modic type 1 vertebral endplate change were large in all three vertebral bodies with false-positive findings. Two of the vertebral bodies showed a significant decrease in height, while the height of the other vertebral body was generally normal. Previous studies have attributed Modic type 1 vertebral endplate changes to traumatic injury to the vertebral endplate (27), localized actions of proinflammatory mediators (28), and, more recently, to low-grade bacterial infection (29). Therefore, similar to BME, Modic type 1 vertebral endplate changes are hypointense on T1-weighted images, hyperintense on

T2-weighted images, and hyperintense on fat-suppressed T2-weighted images. On water-HAP images, Modic type 1 vertebral endplate changes are caused by a high-water concentration that is similar to traumatic BME. Four false-negative findings were associated with minimal BME, resulting in only a slightly high signal on fat-suppressed T2-weighted images that could be easily overlooked. Two of them showed a significant decrease in height while the other two had a normal height. One older adult female patient had mild traumatic back pain for 1 week. MRI identified traumatic BME in three vertebral bodies, with significant edema in two of them which was clearly displayed on DECT; however, the other vertebral body with normal height and mild edema detected by MRI produced a false-negative finding on DECT.

Certain limitations to this study should be acknowledged. First, we did not stratify our study population by bone mineral density (BMD), as we believed that the BMD could have impacted the threshold obtained in our research. In our study, significant differences in water concentration of the normal vertebral bodies were observed between younger (≤50 years old) and older adults (>50 years old) (986.2 *vs.* 875.9 mg/cm^3; P<0.001), which suggests that the critical water concentration for diagnosing vertebral fractures may differ between younger and older individuals. A stratified analysis based on the BMD is needed in future studies. Second, we excluded patients with spinal tumors, spinal infections, and diseases that could affect calcium metabolism. The abnormal changes in bone marrow composition of these individuals should be examined in subsequent research.

Conclusions

The fast kVp-switching DECT water-HAP decomposition technique had an excellent diagnostic performance in distinguishing acute VCFs from chronic ones both in visual and quantitative analyses. The BME areas depicted on DECT and MRI were nearly identical. This confirms the reliability of the water-HAP decomposition technique in the diagnosis of VCF. It is recommended that in emergency situations, DECT inspection should be the first choice if DECT devices are available, especially for older adults.

Acknowledgments

A section of the manuscript has been accepted as a poster presentation at the 109th Scientific Assembly and Annual Meeting of the Radiological Society of North America, to be held November 26–30 in Chicago, Illinois.

Footnote

Reporting Checklist: The authors have completed the STARD reporting checklist. Available at https://qims.amegroups.com/article/view/10.21037/qims-24-1576/rc

Funding: This project was supported by Nanjing Medical Science and Technology Development Fund (No. ZKX23064).

Conflicts of Interest: All authors have completed the ICMJE uniform disclosure form (available at https://qims.amegroups.com/article/view/10.21037/qims-24-1576/coif). All authors report this project was supported by the Nanjing Medical Science and Technology Development Fund (No. ZKX23064). The authors have no other conflicts of interest to declare.

Ethical Statement: The authors are accountable for all aspects of the work in ensuring that questions related to the accuracy or integrity of any part of the work are appropriately investigated and resolved. This retrospective study was conducted in accordance with the Declaration of Helsinki (as revised in 2013) and was approved by the institutional ethics committee of the Affiliated BenQ Hospital of Nanjing Medical University (No. 2023-KL017). The requirement for written informed consent was waived due to the retrospective nature of the analysis.

References

1. Alsoof D, Anderson G, McDonald CL, Basques B, Kuris E, Daniels AH. Diagnosis and Management of Vertebral Compression Fracture. Am J Med 2022;135:815-21.
2. Kaup M, Wichmann JL, Scholtz JE, Beeres M, Kromen

W, Albrecht MH, Lehnert T, Boettcher M, Vogl TJ, Bauer RW. Dual-Energy CT-based Display of Bone Marrow Edema in Osteoporotic Vertebral Compression Fractures: Impact on Diagnostic Accuracy of Radiologists with Varying Levels of Experience in Correlation to MR Imaging. Radiology 2016;280:510-9.
3. Madassery S. Vertebral Compression Fractures: Evaluation and Management. Semin Intervent Radiol 2020;37:214-9.
4. McDonald CL, Alsoof D, Daniels AH. Vertebral Compression Fractures. R I Med J (2013) 2022;105:40-5.
5. Strickland CD, DeWitt PE, Jesse MK, Durst MJ, Korf JA. Radiographic assessment of acute vs chronic vertebral compression fractures. Emerg Radiol 2023;30:11-8.
6. Mandalia V, Fogg AJ, Chari R, Murray J, Beale A, Henson JH. Bone bruising of the knee. Clin Radiol 2005;60:627-36.
7. Abbassi M, Jain A, Shin D, Arasa CA, Li B, Anderson SW, LeBedis CA. Quantification of bone marrow edema using dual-energy CT at fracture sites in trauma. Emerg Radiol 2022;29:691-6.
8. Akisato K, Nishihara R, Okazaki H, Masuda T, Hironobe A, Ishizaki H, Shota K, Yamaguchi H, Funama Y. Dual-Energy CT of Material Decomposition Analysis for Detection with Bone Marrow Edema in Patients with Vertebral Compression Fractures. Acad Radiol 2020;27:227-32.
9. Bierry G, Venkatasamy A, Kremer S, Dosch JC, Dietemann JL. Dual-energy CT in vertebral compression fractures: performance of visual and quantitative analysis for bone marrow edema demonstration with comparison to MRI. Skeletal Radiol 2014;43:485-92.
10. Cavallaro M, D'Angelo T, Albrecht MH, Yel I, Martin SS, Wichmann JL, Lenga L, Mazziotti S, Blandino A, Ascenti G, Longo M, Vogl TJ, Booz C. Comprehensive comparison of dual-energy computed tomography and magnetic resonance imaging for the assessment of bone marrow edema and fracture lines in acute vertebral fractures. Eur Radiol 2022;32:561-71.
11. Diekhoff T, Engelhard N, Fuchs M, Pumberger M, Putzier M, Mews J, Makowski M, Hamm B, Hermann KA. Single-source dual-energy computed tomography for the assessment of bone marrow oedema in vertebral compression fractures: a prospective diagnostic accuracy study. Eur Radiol 2019;29:31-9.
12. Diekhoff T, Hermann KG, Pumberger M, Hamm B, Putzier M, Fuchs M. Dual-energy CT virtual non-calcium technique for detection of bone marrow edema in patients with vertebral fractures: A prospective feasibility study on a single- source volume CT scanner. Eur J Radiol 2017;87:59-65.
13. Engelhard N, Hermann KG, Greese J, Fuchs M, Pumberger M, Putzier M, Diekhoff T. Single-source dual-energy computed tomography for the detection of bone marrow lesions: impact of iterative reconstruction and algorithms. Skeletal Radiol 2020;49:765-72.
14. Foti G, Beltramello A, Catania M, Rigotti S, Serra G, Carbognin G. Diagnostic accuracy of dual-energy CT and virtual non-calcium techniques to evaluate bone marrow edema in vertebral compression fractures. Radiol Med 2019;124:487-94.
15. Jeong SY, Jeon SJ, Seol M, Ahn TH, Juhng SK. Diagnostic performance of dual-energy computed tomography for detection of acute spinal fractures. Skeletal Radiol 2020;49:1589-95.
16. Karaca L, Yuceler Z, Kantarci M, Çakır M, Sade R, Calıkoglu C, Ogul H, Bayrakturan UG. The feasibility of dual-energy CT in differentiation of vertebral compression fractures. Br J Radiol 2016;89:20150300.
17. Neuhaus V, Lennartz S, Abdullayev N, Große Hokamp N, Shapira N, Kafri G, Holz JA, Krug B, Hellmich M, Maintz D, Borggrefe J. Bone marrow edema in traumatic vertebral compression fractures: Diagnostic accuracy of dual-layer detector CT using calcium suppressed images. Eur J Radiol 2018;105:216-20.
18. Pan J, Yan L, Gao H, He Y, Zhong Z, Li P, Zhang Y, Guo Y, Liao L, Zhou S, Zhang K. Fast kilovoltage (KV)-switching dual-energy computed tomography hydroxyapatite (HAP)-water decomposition technique for identifying bone marrow edema in vertebral compression fractures. Quant Imaging Med Surg 2020;10:604-11.
19. Petritsch B, Kosmala A, Weng AM, Krauss B, Heidemeier A, Wagner R, Heintel TM, Gassenmaier T, Bley TA. Vertebral Compression Fractures: Third-Generation Dual-Energy CT for Detection of Bone Marrow Edema at Visual and Quantitative Analyses. Radiology 2017;284:161-8.
20. Schwaiger BJ, Gersing AS, Hammel J, Mei K, Kopp FK, Kirschke JS, Rummeny EJ, Wörtler K, Baum T, Noël PB. Three-material decomposition with dual-layer spectral CT compared to MRI for the detection of bone marrow edema in patients with acute vertebral fractures. Skeletal Radiol 2018;47:1533-40.
21. Wang CK, Tsai JM, Chuang MT, Wang MT, Huang KY, Lin RM. Bone marrow edema in vertebral compression fractures: detection with dual-energy CT. Radiology 2013;269:525-33.

22. Wong AJN, Wong M, Kutschera P, Lau KK. Dual-energy CT in musculoskeletal trauma. Clin Radiol 2021;76:38-49.
23. Liao EY, Wu XP, Luo XH, Zhang H, Dai RC, Huang G, Wang WB. Establishment and evaluation of bone mineral density reference databases appropriate for diagnosis and evaluation of osteoporosis in Chinese women. J Bone Miner Metab 2003;21:184-92.
24. Mandalia V, Henson JH. Traumatic bone bruising--a review article. Eur J Radiol 2008;67:54-61.
25. Pham T, Azulay-Parrado J, Champsaur P, Chagnaud C, Legré V, Lafforgue P. "Occult" osteoporotic vertebral fractures: vertebral body fractures without radiologic collapse. Spine (Phila Pa 1976) 2005;30:2430-5.
26. Chen J, Qiu Z, Jiang N, Xia Y, Li H, Chen S, Liu J, Xue Y. Detecting bone marrow infiltration in nonosteolytic multiple myeloma through separation of hydroxyapatite via the two-material decomposition technique in spectral computed tomography. Quant Imaging Med Surg 2024;14:2345-56.
27. Modic MT, Steinberg PM, Ross JS, Masaryk TJ, Carter JR. Degenerative disk disease: assessment of changes in vertebral body marrow with MR imaging. Radiology 1988;166:193-9.
28. Burke JG, Watson RW, McCormack D, Dowling FE, Walsh MG, Fitzpatrick JM. Intervertebral discs which cause low back pain secrete high levels of proinflammatory mediators. J Bone Joint Surg Br 2002;84:196-201.
29. Albert HB, Lambert P, Rollason J, Sorensen JS, Worthington T, Pedersen MB, Nørgaard HS, Vernallis A, Busch F, Manniche C, Elliott T. Does nuclear tissue infected with bacteria following disc herniations lead to Modic changes in the adjacent vertebrae? Eur Spine J 2013;22:690-6.

Cite this article as: Yao R, Zhu X, Zhou D, Yang L, Yu H, Zhang R, Yu T, Yang M. Fast kilovoltage peak-switching dual-energy computed tomography water-hydroxyapatite decomposition for detecting vertebral compression fracture-related bone marrow edema: a comparison with magnetic resonance imaging. Quant Imaging Med Surg 2025;15(3):2270-2279. doi: 10.21037/qims-24-1576

